Chapter 15
On the Influence of Poisson's Ratio on Phase Transformations Limiting Surfaces

Alexander B. Freidin and Leah L. Sharipova

Abstract The influence of the sign and value of Poisson's ratios of the phases on the limiting surfaces of stress-induced phase transformations is studied. Relationships defining the limiting surfaces in the case of auxetic phases are derived and the difference with the case of positive Poisson's ratio is highlighted. Limiting surfaces for phase transformations in the cases if one or both phases are auxetic materials are compared with the limiting surfaces constructed for 'normal' phases.

Key words: Stress-induced phase transformations · Limiting phase transformation surfaces · Metamaterials · Negative Poisson ratio · Auxetics

15.1 Introduction

Poisson's ratio of a material is defined for a material undergoing tension as the ratio of the lateral contractile strain to the longitudinal tensile strain, i.e., it characterizes, for example, how much a cylindrical specimen becomes thinner or thicker if it is stretched. Most of materials have positive Poisson's ratio. Materials and structures with negative Poisson's ratio (NPR) exhibit a counter-intuitive behaviour. Under uniaxial compression (tension), these materials and structures contract (expand) transversely. Such materials and structures are termed auxetics.

The possibility of negative Poisson's ratio was pointed out by Love [1], who reported $\nu = -1/7$ for some directions in an anisotropic crystal of iron pyrites. In 1985, Kolpakov [2] and Almgren [3] described a material with NPR theoretically. Lakes [4] was apparently the first who produced in 1987 a re-entrant foam structure

Alexander B. Freidin · Leah L. Sharipova
Institute for Problems in Mechanical Engineering RAS, Bolshoy pr., 61, V.O., St. Petersburg, 199178, Russian Federation,
e-mail: alexander.freidin@gmail.com, sleah07@gmail.com

H. Altenbach et al. (eds.), *Sixty Shades of Generalized Continua*,
Advanced Structured Materials 170, https://doi.org/10.1007/978-3-031-26186-2_15

which exhibited NPR. Four years latter, materials with NPR were named ‘auxetics’ or ‘auxetic materials’ by Evans et al. [5].

Auxetics possess better mechanical properties if to compare to conventional materials, such as enhanced indentation resistance [6], bending stiffness and shear resistance [7], high dissipated energy per unit volume under compressive cyclic loading [8]-[10] (see also reviews [11]-[17] and monographs [18]-[22]).

Among the fields of application of auxetics, one can mention medical applications [23]-[26], use in materials for sports equipment [27, 28], in the development of new textile fabrics [29, 30] Also the interest to such materials is motivated by intensive developing new technologies of their creation, particulary on the base of 3D printing [31]-[33].

Nowadays, metamaterials, including auxetics, are also the subject of many theoretical studies, see, e.g., monograph [34], papers [35]-[41] and reference therein. In the present paper we will focus on phase transformations associated with auxetics.

Phase transformations from normal material to auxetic are observed in auxetic foams [42]. The foam specimens were transformed from a state with conventional Poisson’s ratio to auxetic, returned to conventional and once again to auxetic under multiple mechanical and thermal loading. The phase transition from the normal to the auxetic state was also revealed using molecular dynamics modeling [43] and in an experiment on carbon honeycombs [44].

Earlier we have developed a procedure for the construction of limiting phase transformations surfaces in a strain space for stress-induced phase transformations [45]-[47]. The phase transformation cannot start until the limiting surface is achieved on a given straining path, analogously to the yield surface in plasticity theory. There are two limiting surfaces in the case of a phase transformation: for direct and reverse transformations, and stress-strain diagrams on the transformation pathes were constructed. During these studies, the problems of optimal composite microstructures were also solved: given average strain a minimizing microstructure was found and corresponding energy was derived (see also [48]-[50]). But at that time only the case of positive Poisson’s ratios of the phases was implied in derivations.

In the present paper we study in detail how the formulae defining the transformation surfaces and the shapes of the surfaces are changed depending on the sign and value of Poisson’s ratios of the phases. Various combinations of the signs of Poisson’s ratios of the phases are considered.

The paper is arranged as follows. In Sect. 15.2 we recall the notions of phase equilibrium and phase transition zones and derive the relationships for the construction of phase transition zones in the case of negative Poisson’s ratio, highlighting the difference with the case of positive Poisson’s ratio.

In Sect. 15.3 we summarize the results on optimal laminates, minimizing microstructures obtained in [45]-[47] and discuss how to construct the phase transformations limiting surfaces in the case of arbitrary Poisson’s ratio, including the negative ratio. In Sect. 15.4 phase transformation limiting surfaces for phase transformations ‘auxetic $\leftrightarrow$ normal material’ and ‘auxetic $\leftrightarrow$ auxetic’ are constructed and compared with the limiting surface for the case of phases with positive Poisson’s

ratio. Section 15.5 contains conclusions. In Appendix the formulae related to the construction of the limiting surfaces are derived.

15.2 Phase Equilibrium and Phase Transition Zones for Phases with Positive and Negative Poisson's Ratios

The notion of phase transition zones (PTZ) appeared as a result of the analysis of the conditions across an equilibrium phase boundary (an interface) in an elastic solid [51]-[53]. The PTZ is formed in a strain space by all deformations that can exist at the equilibrium interfaces in a given material, whatever the loading conditions.

The usefulness of the PTZ construction can be motivated as follows

- PTZ is defined exclusively by the material properties (elasticity moduli of the phases, transformation strain) and the energy parameter defined by the temperature.
- Each point of the PTZ boundary corresponds to some piecewise homogeneous two - phase configuration with a plane interface. The external boundaries of the PTZ can be considered as the limiting surfaces of the nucleation of layers of a new phase. The PTZ represents locally all possible equilibrium interfaces.
- The PTZ construction may be related with the interface stability analysis. For elastic solids, it was shown that instability of the interface was not observed if deformations at the interface coincided with deformations at the external boundaries of the PTZ[54]-[56]. Then it was proved that belonging the deformations at the interface to the external boundaries of the PTZ is a necessary stability condition [57, 58].
- Even if a new phase appears in a more complex form than simple layers, in order to construct the phase transformations limiting surfaces, it is necessary to find the maximum of the quadratic form, which is examined when constructing the PTZ [45]-[47].

In the case of small strains, the construction of the PTZ was considered for the general case of isotropic phases but implemented for positive Poisson's coefficients of phases (see, e.g., [52, 53], [59]-[61]. The result with positive Poisson's ratio were used also in finding energy minimizing microstructures and construction of phase transformations limiting surfaces [45]-[47]. In the present paper we focus on the case of negative Poisson's ratio. For the sake of completeness, we repeat briefly some general derivations and results.

In the case of small strains a problem on equilibrium two-phase configurations of elastic bodies is reduced to finding the interface Γ and corresponding displacement field $\boldsymbol{u}(\boldsymbol{x})$, which is smooth enough at material points $\boldsymbol{x} \notin \Gamma$, continuous across Γ

$$[[\boldsymbol{u}]] = 0, \quad \boldsymbol{x} \in \Gamma \tag{15.1}$$

and satisfies boundary conditions and equilibrium conditions

$$\boldsymbol{x} \notin \Gamma: \quad \nabla \cdot \boldsymbol{\sigma} = 0, \tag{15.2}$$

$$\boldsymbol{x} \in \Gamma: \quad [[\boldsymbol{\sigma}]] \cdot \boldsymbol{n} = 0, \quad [[f]] - \langle \boldsymbol{\sigma} \rangle : [[\boldsymbol{\varepsilon}]] = 0, \tag{15.3}$$

where $\boldsymbol{n}$ is the unit normal to the boundary, $\boldsymbol{\sigma}$ and $\boldsymbol{\varepsilon} = (\nabla \boldsymbol{u} + \nabla \boldsymbol{u}^T)/2$ are the stress and strain tensors, square and angle brackets denote the jump across the interface and arithmetic mean: $[[a]] = a_+ - a_-$, $\langle a \rangle = 1/2(a_+ + a_-)$, subscripts "–" and "+" refer the values to a material being in the "–" and "+" phase states, respectively.

Thermodynamic condition $(15.3)_2$ follows from the conditions on the equilibrium phase boundary in a nonlinear elastic material, see [62] and reference therein. Note that from displacement and traction continuity it follows that

$$\langle \boldsymbol{\sigma} \rangle : [[\boldsymbol{\varepsilon}]] = \boldsymbol{\sigma}_+ : [[\boldsymbol{\varepsilon}]] = \boldsymbol{\sigma}_- : [[\boldsymbol{\varepsilon}]].$$

The volume density of the Helmholtz free energy is taken in a form

$$f(\boldsymbol{\varepsilon}) = \min_{-,+} \left\{ f^-(\boldsymbol{\varepsilon}), f^+(\boldsymbol{\varepsilon}) \right\} \tag{15.4}$$

where the energies of the phases are

$$f_\pm(\boldsymbol{\varepsilon}) = f_\pm^0 + w_\pm(\boldsymbol{\varepsilon}), \quad w_\pm(\boldsymbol{\varepsilon}) = \frac{1}{2}(\boldsymbol{\varepsilon} - \boldsymbol{\varepsilon}_\pm^*) : \boldsymbol{C}_\pm : (\boldsymbol{\varepsilon} - \boldsymbol{\varepsilon}_\pm^*), \tag{15.5}$$

$w_\pm(\boldsymbol{\varepsilon})$ are the strain energies, $\boldsymbol{C}_\pm$ are the elasticity tensors, $f_\pm^0$ are the chemical energies of the phases defined by the temperature, $\boldsymbol{\varepsilon}_\pm^*$ are the strains in stress-free states; if one of the strains $\boldsymbol{\varepsilon}_\pm^*$ is zero then another one is the transformation strain $\boldsymbol{\varepsilon}^{tr}$.

Constitutive equations take the form

$$\boldsymbol{\sigma}_\pm(\boldsymbol{\varepsilon}) = \boldsymbol{C}_\pm : \left(\boldsymbol{\varepsilon} - \boldsymbol{\varepsilon}_\pm^*\right), \quad \boldsymbol{\varepsilon} \in \mathcal{E}_\pm \tag{15.6}$$

where domains of definition of phases "–" and "+"

$$\mathcal{E}_- = \{\boldsymbol{\varepsilon}: \ \psi(\boldsymbol{\varepsilon}) > 0\}, \ \mathcal{E}_+ = \{\boldsymbol{\varepsilon}: \ \psi(\boldsymbol{\varepsilon}) < 0\}, \qquad \psi(\boldsymbol{\varepsilon}) = f^+(\boldsymbol{\varepsilon}) - f^-(\boldsymbol{\varepsilon}). \tag{15.7}$$

It follows from $(15.3)_1$, (15.6) and (15.1) that [63]

$$[[\boldsymbol{\varepsilon}]] = -\boldsymbol{K}_\mp(\boldsymbol{n}) : \boldsymbol{q}_\pm, \quad \boldsymbol{q}_\pm = [[\boldsymbol{C}]] : \boldsymbol{\varepsilon}_\pm - [[\boldsymbol{C} : \boldsymbol{\varepsilon}^*]], \qquad \boldsymbol{K}_\pm(\boldsymbol{n}) = \{\boldsymbol{n} \otimes \boldsymbol{G}_\pm \otimes \boldsymbol{n}\}^s, \ \boldsymbol{G}_\pm = (\boldsymbol{n} \cdot \boldsymbol{C}_\pm \cdot \boldsymbol{n})^{-1}, \tag{15.8}$$

s means the symmetrization: $K_{ijkl} = n_{(i} G_{j)(k} n_{l)}$.

Substituting (15.5), (15.6) into $(15.3)_2$ and using (15.8) leads to the thermodynamic equilibrium condition in the forms [64]

$$2\gamma + [[\boldsymbol{\varepsilon}^* : \boldsymbol{C} : \boldsymbol{\varepsilon}^*]] + \boldsymbol{\varepsilon}_\pm : [[\boldsymbol{C}]] : \boldsymbol{\varepsilon}_\pm - 2\boldsymbol{\varepsilon}_\pm : [[\boldsymbol{C} : \boldsymbol{\varepsilon}^*]] \pm \boldsymbol{q}_\pm : \boldsymbol{K}_\mp(\boldsymbol{n}) : \boldsymbol{q}_\pm = 0 \tag{15.9}$$

where upper and lower signs and indices '+" and "–" correspond to each other, $\gamma = [[f_0]]$ acts as temperature in absence of thermal stresses.

Any of two equations (15.9) determines one-parametric family of unit normals depending on γ and strains on one side ("+" or "−") of the interface. Those $\boldsymbol{\varepsilon}_-$ and $\boldsymbol{\varepsilon}_+$ at which the equation is solvable for the unit normal form a phase transition zone in strain space that consists of two subzones $\mathcal{E}_-$ and $\mathcal{E}_+$ [52, 53, 59, 60].

If the inverse tensor $[[\boldsymbol{C}]]^{-1}$ exists, then (15.9) can be rewritten in terms of $\boldsymbol{q}$ as

$$\varphi(\boldsymbol{q}_\pm) \pm \mathcal{K}_\mp(\boldsymbol{q}_\pm, \boldsymbol{n}) = 0, \tag{15.10}$$

$$\varphi(\boldsymbol{q}_\pm) = 2\gamma_* + \boldsymbol{q}_\pm : [[\boldsymbol{C}]]^{-1} : \boldsymbol{q}_\pm, \quad \mathcal{K}_\mp(\boldsymbol{q}_\pm, \boldsymbol{n}) = \boldsymbol{q}_\pm : \boldsymbol{K}_\mp(\boldsymbol{n}) : \boldsymbol{q}_\pm,$$

$$\gamma_* = \gamma + \frac{1}{2}[[\boldsymbol{\varepsilon}^*]] : [[\boldsymbol{B}]]^{-1} : [[\boldsymbol{\varepsilon}^*]], \quad \boldsymbol{B}_\pm = \boldsymbol{C}_\pm^{-1}$$

Tensors $\boldsymbol{q}$ for which Eqs. (15.10) can be solved for the unit normal $\boldsymbol{n}$ form the phase transition zone in q-space that consists of two subzones $\mathcal{Q}_\pm$. The subzones $\mathcal{Q}_\pm$ and corresponding subzones $\mathcal{E}_\pm$ are defined by inequalities

$$\mathcal{K}_\mp^{\min}(\boldsymbol{q}_\pm) \le \mp\varphi(\boldsymbol{q}_\pm) \le \mathcal{K}_\mp^{\max}(\boldsymbol{q}_\pm), \tag{15.11}$$

$$\mathcal{K}_\mp^{\max}(\boldsymbol{q}_\pm) = \max_{\boldsymbol{n}} \mathcal{K}_\mp(\boldsymbol{q}, \boldsymbol{n}), \quad \mathcal{K}_\mp^{\min}(\boldsymbol{q}_\pm) = \min_{\boldsymbol{n}} \mathcal{K}_\mp(\boldsymbol{q}_\pm, \boldsymbol{n}),$$

The normals

$$\boldsymbol{n}_{\text{ex}}^\pm(\boldsymbol{q}) = \arg\max_{\boldsymbol{n}} \mathcal{K}_\mp(\boldsymbol{q}, \boldsymbol{n}), \quad \boldsymbol{n}_{\text{in}}^\pm(\boldsymbol{q}) = \arg\min_{\boldsymbol{n}} \mathcal{K}_\mp(\boldsymbol{q}, \boldsymbol{n}) \tag{15.12}$$

to the interface correspond to external and internal boundaries of the subzones $\mathcal{Q}_\pm$ and $\mathcal{E}_\pm$ [52, 53].

The external boundaries of the subzones are given by the equations

$$\varphi(\boldsymbol{q}_+) + \mathcal{K}_-^{\max}(\boldsymbol{q}_+) = 0, \quad \mathcal{K}_+^{\max}(\boldsymbol{q}_-) - \varphi(\boldsymbol{q}_-) = 0. \tag{15.13}$$

The internal boundaries are given by the equations

$$\varphi(\boldsymbol{q}_+) + \mathcal{K}_-^{\min}(\boldsymbol{q}_+) = 0, \quad \mathcal{K}_+^{\min}(\boldsymbol{q}_-) - \varphi(\boldsymbol{q}_-) = 0. \tag{15.14}$$

The surface dividing the domains of definition of the phases, i.e. corresponding to (15.8), passes between the internal boundaries (15.14). Note that in relationships (15.10)–(15.14) tensors $\boldsymbol{\varepsilon}_\pm^*$ related to the transformation strain are hidden in $\boldsymbol{q}$ and parameter γ_*.

Further we consider isotropic phases with the elasticity tensors

$$\boldsymbol{C}_\pm = \lambda_\pm \boldsymbol{E} \otimes \boldsymbol{E} + 2\mu_\pm \boldsymbol{I}, \tag{15.15}$$

where $\lambda_\pm$ and $\mu_\pm$ are Lamé's coefficients, $\boldsymbol{E}$ and $\boldsymbol{I}$ are the second and forth rank unit tensors, in Cartesian coordinates $E_{ij} = \delta_{ij}$,

$$I_{ijkl} = \frac{1}{2}(\delta_{ik}\delta_{jl} + \delta_{il}\delta_{jk}),$$

δ_{ij} is Kroneker's delta. Then

$$\boldsymbol{K}_{-}(\boldsymbol{n}) = \frac{1}{\mu_{-}}\left((\boldsymbol{n}\otimes\boldsymbol{E}\otimes\boldsymbol{n})^{s} - a_{-}\boldsymbol{n}\otimes\boldsymbol{n}\otimes\boldsymbol{n}\otimes\boldsymbol{n}\right) \tag{15.16}$$

$$\mathcal{K}_{-}(\boldsymbol{q}_{+},\boldsymbol{n}) = \frac{1}{\mu_{-}}F(N_1,N_2), \tag{15.17}$$

where $F(N_1,N_2) = N_2 - aN_1^2$, $a = (2(1-\nu_{-}))^{-1}$, ν_{-} is Poisson's ratio, $N_1 = \boldsymbol{n}\cdot\boldsymbol{q}_{+}\cdot\boldsymbol{n}$ and $N_2 = \boldsymbol{n}\cdot\boldsymbol{q}_{+}^2\cdot\boldsymbol{n}$ are the orientation invariants.

Representation (15.17) admits the following geometrical interpretation of the equation (15.10) and inequalities (15.11) (Fig. 15.1). Given $\boldsymbol{q}_{+}$, (15.10) takes the form of a relationship between orientation invariants

$$N_2 = aN_1^2 - \mu_{-}\varphi(\boldsymbol{q}_{+}) \tag{15.18}$$

which defines a parabola on N_1N_2-plane. Note that $0 < a \le 1$ if $\nu \le 0.5$.

Since a couple of orientation invariants N_1, N_2 has to determine the unit normal $\boldsymbol{n}$, there are restrictions on N_1, N_2. In the basis of eigenvectors of $\boldsymbol{q}_{+} = \sum q_i\boldsymbol{e}_i\otimes\boldsymbol{e}_i$ the normal is determined by the system of linear equations for $p_i = n_i^2$ ($n_i = \boldsymbol{n}\cdot\boldsymbol{e}_i$, i=1,2,3)

$$\sum p_i = 1, \quad \sum q_i p_i = N_1, \quad \sum q_i^2 p_i = N_2 \tag{15.19}$$

Since the solution of system (15.19) is to be non–negative, the admissible values domain $\mathcal{D}$ for orientation invariants N_1, N_2 is a triangle with vertexes (q_i, q_i^2) $(i = 1,2,3)$ (see Fig. 15.1). The vertexes correspond to $\boldsymbol{n} = \boldsymbol{e}_i$, points of ij-side

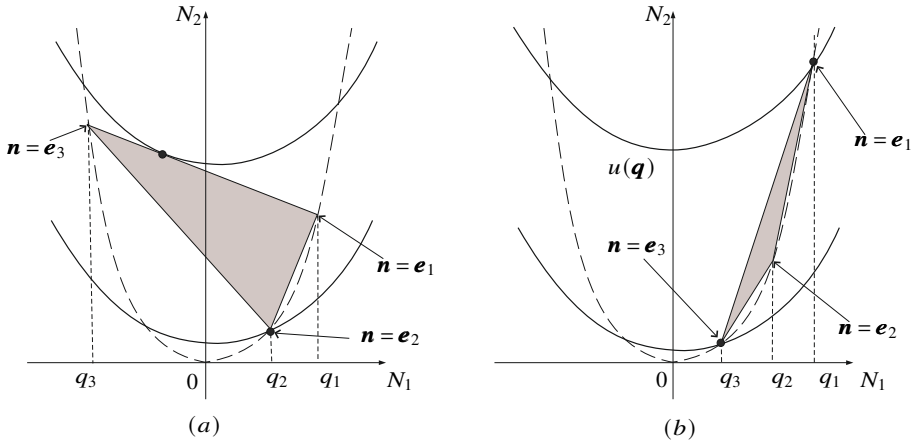

Fig. 15.1: Domains (triangles) of admissible values of orientation invariants and limiting curves of the one-parametric family of solution: (a) - parabola touches the side corresponding to the maximal and minimal eigenvalues of the tensor $\boldsymbol{q}$ (b) - parabola (15.18) passes through vertexes of the triangle.

of the triangle correspond to normal $\boldsymbol{n}$ lying in the ij-principal plane of $\boldsymbol{q}_+$. If q_i $(i = 1, 2, 3)$ change, then vertexes of $\mathcal{D}$ move along the skeleton curve $N_2 = N_1^2$.

On the other hand, the parabola (15.18) moves along N_2-axis if $\boldsymbol{q}_+$ changes. The line of intersection of the parabola and $\mathcal{D}$ gives one parameter family of solutions. The subzone Q_+ is formed by all $\boldsymbol{q}_+$ such that this intersection exists.

One can see that, depending on the eigenvalues of $\boldsymbol{q}_+$, the maximum value corresponds to the point where the parabola touches the upper side of the triangle, corresponding to maximal and minimal eigenvalues (Fig. 15.1(a), the normal lies in the corresponding eigenplane in tis case), or passes via the vertex corresponding to the eiginvalue, having the maximal absolute value (Fig. 15.1(b), the normal coinsides with the corresponding eigenvector).

The minimal value correspond to passing the parabola via the vertex corresponding to the eiginvalue with the minimal absolute value, the normal coinsides with the corresponding eigenvector.

The above considerations can be formalized as follows (see also Appendix):

1. Assume that the tensor $\boldsymbol{q}_+$ has different eigenvalues, and $q_{\min}$, $q_{\max}$ and q_{mid}, and $\boldsymbol{e}_{\max}$, $\boldsymbol{e}_{\min}$ and $\boldsymbol{e}_{\mathrm{mid}}$ are the minimal, maximal and intermediate eigenvalues and corresponding eigenvectors of $\boldsymbol{q}_+$; $n_{\min}$, $n_{\max}$ and n_{mid} are components of the normal $\boldsymbol{n}$ in the basis of eigenvectors of $\boldsymbol{q}_+$, $|q|_{\max}$ and $|q|_{\min}$ are the maximal and minimal absolute values of the eigenvalues, $\boldsymbol{e}_{|q|\max}$ and $\boldsymbol{e}_{|q|\min}$ are the corresponding eigenvectors.
   If $\nu_- > 0$ and

$$q_{\min}q_{\max} < 0 \quad \text{or} \quad \begin{cases} q_{\min}q_{\max} > 0 \\ (1-\nu_-)|q|_{\min} < \nu_-|q|_{max}. \end{cases} \tag{15.20}$$

   or $\nu_- < 0$ and

$$\begin{cases} q_{\min}q_{\max} < 0 \\ (1-\nu_-)|q|_{\min} + \nu_-|q|_{\max} > 0. \end{cases} \tag{15.21}$$

   then the normal $\boldsymbol{n}^+_{\mathrm{ex}}$ to the intertface corresponding to the external PTZ boundary lies in the plane of maximal and minimal eigenvalues of $\boldsymbol{q}_+$: $n_{\mathrm{mid}} = 0$,

$$n^2_{\max} = \frac{(1-\nu_-)q_{\max} - \nu_- q_{\min}}{q_{\max} - q_{\min}}, \quad n^2_{\min} = \frac{\nu_- q_{\max} - (1-\nu_-)q_{\min}}{q_{\max} - q_{\min}}, \tag{15.22}$$

   Then for both $\nu_- > 0$ and $\nu_- < 0$

$$\mathcal{K}^{\max}_- = \frac{1-\nu_-}{2\mu_-}(q^2_{\max} + q^2_{\min}) - \frac{\nu_-}{\mu_-}q_{\max}q_{\min}. \tag{15.23}$$

   If conditions (15.20) for $\nu_- > 0$ or (15.21) for $\nu_- < 0$ are not satisfied then

$$\boldsymbol{n}^+_{ex} = \boldsymbol{e}_{|q|\max}, \quad \mathcal{K}^{\max}_- = \frac{1-2\nu_-}{2\mu_-(1-\nu_-)}|q|^2_{\max}. \tag{15.24}$$

We emphasize that if $\nu_- < 0$ then only the case $q_{\min} q_{\max} < 0$ with additional restrictions allows normal (15.22) lying in the eigenplane of $\boldsymbol{q}_+$
The normal to the interface corresponding to the internal PTZ boundary and $\mathcal{K}_-^{\min}$ are given by formulae:

$$\boldsymbol{n}_{\text{in}}^{+} = \boldsymbol{e}_{|q|\min}, \quad \mathcal{K}_-^{\min} = \frac{1-2\nu_-}{2\mu_-(1-\nu_-)} |q|^2_{\max}. \tag{15.25}$$

2. Assume that the tensor $\boldsymbol{q}_+$ is axisymmetric:

$$\boldsymbol{q}_+ = q(\boldsymbol{E} - \boldsymbol{k}\otimes\boldsymbol{k}) + q_k \boldsymbol{k}\otimes\boldsymbol{k}.$$

Then the domain $\mathcal{D}$ degenerates into the straight segment with the ends on the skeleton parabola.
If $\nu_- > 0$ and

$$q_k q < 0 \quad \text{or} \quad \begin{cases} q_k q > 0 \\ (1-\nu_-)|q|_{\min} - \nu_- |q|_{\max} < 0. \end{cases} \tag{15.26}$$

or $\nu_- < 0$ and

$$\begin{cases} q_k q < 0 \\ (1-\nu_-)|q|_{\min} + \nu_- |q|_{\max} > 0 \end{cases} \tag{15.27}$$

$$|q|_{\min} = \min\{|q_k|, |q|\}, \quad |q|_{\max} = \max\{|q_k|, |q|\},$$

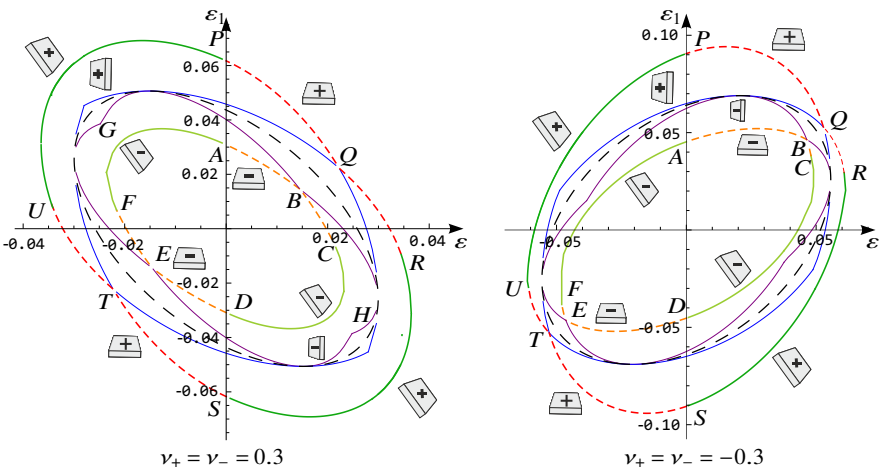

Fig. 15.2: The cross sections of the phase transition zones by the plane $\varepsilon_1 = \varepsilon_2 = \varepsilon$ for a normal materials and for auxetics. Initial undeformed state is phase "+" ($\vartheta^{tr} = 0$).

Table 15.1: Parameters.

Fig.	μ_+	μ_-	ν_+	ν_-	K_+	K_-	λ_+	λ_-	ϑ^{tr}	γ
Fig. 15.4	55	15	-0.3	0.3	16	32.5	-20	22	-0.06	-0.05
Fig. 15.5	55	15	0.3	-0.3	119	4	82	-5	-0.06	-0.05
Fig. 15.2,15.7	30	15	·	·	·	·	·	·	0	-0.05

then the maximum of $\mathcal{K}_-$ is reached at any normal with the square of the projection onto the axe $\boldsymbol{k}$ equal to

$$n_k^2 = \frac{(1-\nu_-)q_k - \nu_- q}{q_k - q}. \tag{15.28}$$

Then

$$\mathcal{K}_-^{\max} = \frac{1-\nu_-}{2\mu_-}(q_k^2 + q^2) - \frac{\nu_-}{\mu_-} q_k q, \tag{15.29}$$

If conditions (15.26), (15.27) are not satisfied then the maximum of $\mathcal{K}_-$

$$\mathcal{K}_-^{max} = \frac{1-2\nu_-}{2\mu_-(1-\nu_-)}|q|^2_{\max} \tag{15.30}$$

is achieved at

$$\begin{aligned} \boldsymbol{n}^* &= \boldsymbol{k} \quad \text{if} \quad |q_k| > |q|, \\ \boldsymbol{n}^* &\perp \boldsymbol{k} \quad \text{if} \quad |q_k| < |q|. \end{aligned}$$

3. Assume that the tensor $\boldsymbol{q}_+$ is spherical: $\boldsymbol{q}_+ = q\boldsymbol{E}$. Then $\mathcal{K}_-$ does not depend on $\boldsymbol{n}$,

$$\boldsymbol{q}_+ : \boldsymbol{K}_-(\boldsymbol{n}) : \boldsymbol{q}_+ = cq^2, \quad c = \frac{1-2\nu_-}{2\mu_-(1-\nu_-)} = \left(k_- + \frac{4}{3}\mu_-\right)^{-1}, \tag{15.31}$$

k_- is the bulk modulus.

The examples of the PTZ cross section by plane $\varepsilon_2 = \varepsilon_3$, constructed by formulae (15.13), (15.14) for the cases $\nu_+ = \nu_- > 0$ and $\nu_+ = \nu_- < 0$ are shown in Fig. 15.2. We take the phase "+" as an initial phase and assume that the transformation strain is spherical. Then $f_+^0 < f_-^0$, $\boldsymbol{\varepsilon}_+^* = 0$, $\boldsymbol{\varepsilon}_-^* = \boldsymbol{\varepsilon}^{tr} = (\vartheta^{tr}/3)\boldsymbol{E}$, i.e. $\gamma < 0$. The parameters are given in Table 15.1. The units are not shown, but Lamé constants and corresponding bulk moduli can be considered as given in GPa. The choice of parameter values was made according to reasons of better visualization of the variety of graphs here and further and consistency with the small strains approach.

In the figures, lines $ABCDEFA$ (direct phase transformation) and $PQRSTUPQ$ (reverse phase transformation) are the external boundaries of the subzones $\mathcal{E}_+$ and $\mathcal{E}_-$, respectively. Lines $BGEHB$ and $QKTLQ$ are the internal PTZ boundaries of the subzones $\mathcal{E}_+$ and $\mathcal{E}_-$.

Dashed black lines, dividing the domains of definition of phases "+" and "−", are determined by the equation $\psi(\boldsymbol{\varepsilon}) = 0$ (see (15.7)).

The parts ABC, FED, PQR, UTS of the external boundaries of the PTZ correspond to the normal, orientation of which coincides with the eigenvector of the tensor $\boldsymbol{q}$ (the interface is perpendicular to an eigenvector of $\boldsymbol{q}$). The parts AF, DC, UP and SR correspond to the normal lying the principal plane of the tensor $\boldsymbol{q}$ (the interface is oriented similar to shear band with the angle depending on the eigenvalues of $\boldsymbol{q}$).

In terms of minimizing laminates (see the next section), ABC and FED are the parts of the limiting surface corresponding to the nucleation of direct first-rank laminates; AF and DC are the parts of the limiting surface corresponding to the nucleation of inclined first-rank laminates.

Note that the external boundary $PQRSTUPQ$ of the subzone $\mathcal{E}_-$ is non-convex. The phase transformations limiting surface construction leads to the convexication with the use of microstructure which are not reduced to simple layers.

One can see that the sign of the Poisson's ratio does not change the expressions of $\mathcal{K}_-^{max}$ but changes the conditions for switching the orientation of the normal. The orientation of the PTZ with respect to strain axes is also changed.

15.3 Optimal Laminates and Phase Transformations Limiting Surfaces

Two phase states, corresponding to the energy minimization may not be limited to simple layers. By the Gibbs principle, at given temperature and average strains, average Helmholtz free energy of a two-phase microstructure

$$F = \int_{\Omega} \left((1 - H(\boldsymbol{x}))\, f_-(\boldsymbol{\varepsilon}) + H(\boldsymbol{x})\, f_+(\boldsymbol{\varepsilon})\right) d\Omega, \tag{15.32}$$

in the case of equilibrium, is to be minimal with respect to the new phase volume fraction and the geometry parameters of the microstructure. Here subscripts "−" and "+" indicate values related to the phases "−" and "+", $\Omega = \Omega_- \bigcup \Omega_+$ is a unit cell divided into subdomains Ω_- and Ω_+ occupied by the phases "−" and "+", $H(\boldsymbol{x})$ is the characteristic function of the subdomain Ω_+:

$$H(\boldsymbol{x}) = \begin{cases} 1, & \boldsymbol{x} \in \Omega_+, \\ 0, & \boldsymbol{x} \in \Omega_-. \end{cases}$$

We take the free energy density in a form (15.4), (15.5), and the constitutive equations in the form (15.6). Consider further the case when the shear module μ_+ of the phase "+" is greater then the shear module of the phase "−", i.e. $\mu_+ > \mu_-$.

It was proved [45] that the infimum of energy (15.32), (15.5) can be constructed with the use of laminates of the first, second and third rank (Fig. 15.3). The formulae for the construction of the phase transformations limiting surface were derived and

then example were done for the case of positive Poisson's ratios [45]–[47]. The construction is based, in particular, on the use of extreme properties of the quadratic form $\mathcal{K}_-(\boldsymbol{q}_+,\boldsymbol{n})$ described in Sect. 15.2.

The first-rank laminate consists of alternating planar layers occupied by homogeneous phases "−" and "+". Then the second-rank laminate consists of alternating layers of the phase "−" and layers which are themselves first-rank laminates. It is characterized by two normals to the layers and sublayers of phase "−" and by an additional parameter related with the volume fraction of the pure layers of the phase "−". The third-rank laminates consists of the layers of the phase "−" and layers which are second-rank laminates. They are characterized by three normals and two additional parameters related with the volume fractions of pure layers of phase "−" and the volume fraction of phase "−" in the included second rank laminates. Note that in the case of the second-rank and third-rank laminates, the phase "+" with greater shear module occupies the inner domains surrounded by the phase "−". The characteristic sizes of the laminates decrease at every step of the microstructure construction and the strains in such layered material tend to piece-wise constant fields, see, e.g., [65].

Five cases ('regimes') were distinguished.

1. Direct first-rank laminates.
   The eigenvalues of $\boldsymbol{q}_+$ are different and do not satisfy conditions (15.20), (15.21). The normal and quadratic forma are defined by Eq. (15.24)
2. Inclined first-rank laminates.
   The eigenvalues of $\boldsymbol{q}_+$ are different and satisfy one the conditons conditons (15.20), (15.21) which depend on the sign of the Poisson ration. The normal and quadratic form are defined by Eq. (15.22), (15.23).
3. Skew second-rank laminates.
   Tensor $\boldsymbol{q}_+$ is axisymmetric. The eigenvalues satisfy conditon (15.26) or (15.27). The quadratic form is defined by Eq. (15.29).

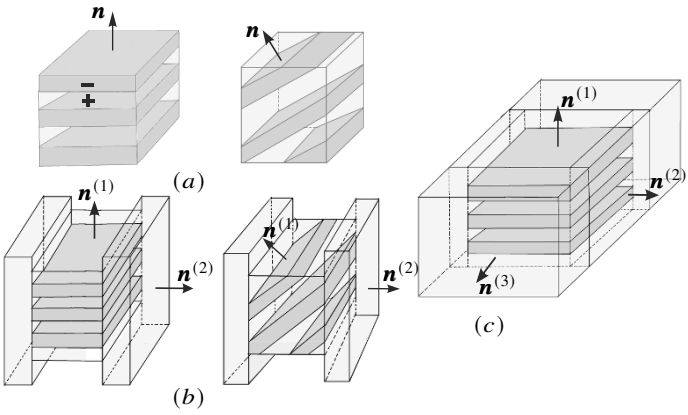

Fig. 15.3: Laminates for optimal microstructures: (a) – direct and inclined first-rank laminates, (b) – direct and skew second-rank laminates, (c) – third-rank laminate.

4. Direct second-rank laminates.
   Tensor $\boldsymbol{q}_+$ is axisymmetric. The eigenvalues do not satisfy conditons (15.26) and (15.27). The quadratic form is defined by Eq. (15.30).
5. Third-rank laminates. Tensor $\boldsymbol{q}_+$ is spherical. The quadratic form is defined by Eq. (15.31).

The external average strain can be related with the tensor $\boldsymbol{q}_+$. Then the limiting surface can be constructed in strain space. Basic relationships and detais of the procedure can be found in [45]-[47]. The influence of Poisson's ratio is highlighted in the next section.

15.4 Results

The cross sections of phase transformation limiting surfaces and surfaces of the appearance of different laminates by the plane $\varepsilon_2 = \varepsilon_3$ are shown in Figs. 15.4, 15.5, 15.7. The parameters taken in calculations are given in Table 15.1.

Materials with positive and negative Poisson's ratios are referred as normal materials and auxetics, respectively. Fig. 15.4 demonstrates the cross-sections for the direct and reverse phase transformations between the auxetic and normal material. Fig. 15.5 represents the cross-sections for the phase transformations if the initial phase state is a normal material which transforms into the auxetic.

Figure 15.6 represents the sketches of the dependencies of the free energy on volume strains: Fig. 15.6(a) corresponds to Fig. 15.4; Fig. 15.6(b) corresponds to Fig. 15.5. Note that in the first case the jump of the elasticity tensor is not sign-definite: the bulk module increases while the shear module decreases due to the phase transformation from the auxetic to the normal material. This leads to unclosed limiting surfaces, as it was mentioned in [45, 59].

Various lines correspond to various types of laminates. Red and orange lines in Figs. 15.4 and 15.5 correspond to the appearance of the direct first-rank laminates, green dashed lines – to skew first-rank laminates, blue dashed lines – to the direct second-rank laminates, black lines – to the skew second-rank laminates, segments AB and $A'B'$ in Fig. 15.4 and segments CD and $C'D'$ in Fig. 15.5 – to the third-rank laminates.

The phase transformations limiting surfaces are given by the combination of the surfaces, corresponding to the appearance of various laminates. Recall that the laminate micrtostructures are mathematical objects allowing to construct energy minimizers and may not be observed in a material. In the case of Fig. 15.4 lines *FOG* represent the limiting surfaces of the transformations from the auxetic to the normal material. Lines *SC'B'A'T* and *SABCT* correspond to the limiting surfaces of the transformations from the normal material to the auxetic.

In the case of Fig. 15.5 the limiting surface of the direct transformation from the normal material to the auxetic is presented by line *PQRS*. The reverse transformation from the auxetic to normal material is presented by line *BCDEB'C'D'E'B*. Dashed black lines divides areas of definition of phases "+" and "−".

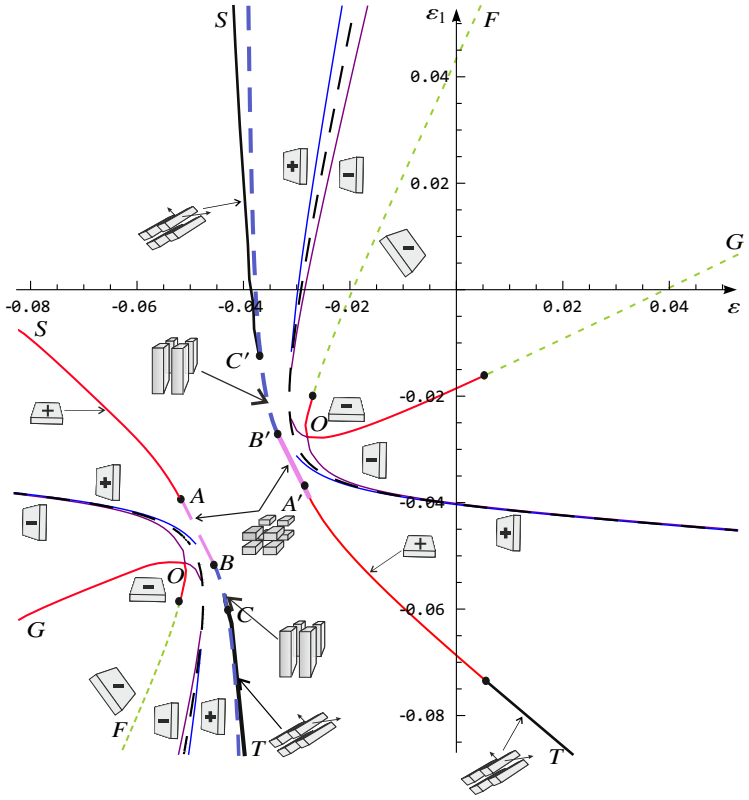

Fig. 15.4: Limiting surface for the phase transformation from the auxetic (phase "+") to normal material (phase "−").

If the energy parameter γ, defined by the temperature, decreases then the limiting surfaces expand and, therefore, the direct phase transformation starts later while the reverse transformation — earlier.

Phase transformations limiting surfaces for various values of Poisson's ratios of the phases in the case of phase transformations between normal phases with equal positive and zero Poisson' ratios and between auxetics with equal negative Poisson's ratios are shown in Fig. 15.7. One can observe that the orientation of the limiting surface with respect to strain axes and its shape are different for positive and negative Poisson' ratios. In the case of positive Poisson's ratio the cross-section is elongated along the axis $\epsilon_1 = -\epsilon_2 = -\epsilon_3$. If $\nu_+ = \nu_- \to 0.5$ then the limiting surface stretches in direction of this axe $\epsilon_1 = \epsilon_2 = \epsilon_3$ and shrinks in the perrpendicular direction. In the case of negative positive Poisson's ratios the cross-section is elongated along the axis $\epsilon_1 = \epsilon_2 = \epsilon_3$. If $\nu_+ = \nu_- \to -1$ then the limiting surface stretches in the direction of the axe $\epsilon_1 = \epsilon_2 = \epsilon_3$ and shrinks in the perpendicular direction.

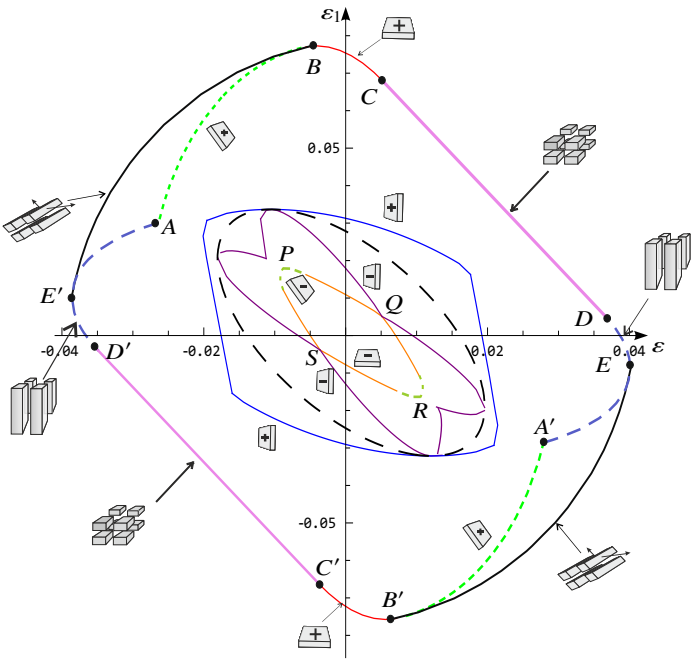

Fig. 15.5: Limiting surfaces for the phase transformation from the normal material (phase "+") to auxetic (phase "−").

15.5 Conclusions

We developed a procedure for the construction of phase transformation limiting surfaces of stress-induced phase transformation – a phase diagram in a strain space – for the case of auxetic phases. Adopting the procedures developed earlier for the case of positive Poisson's ratio, and implementing the approach based on the energy minimizer construction we found minimizing microstructures and derived formulae

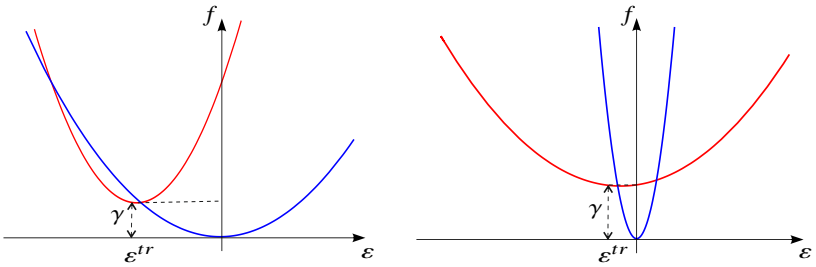

Fig. 15.6: Free energy in the cases corresponding to: (a) – Fig. 15.4; (b) – Fig. 15.5.

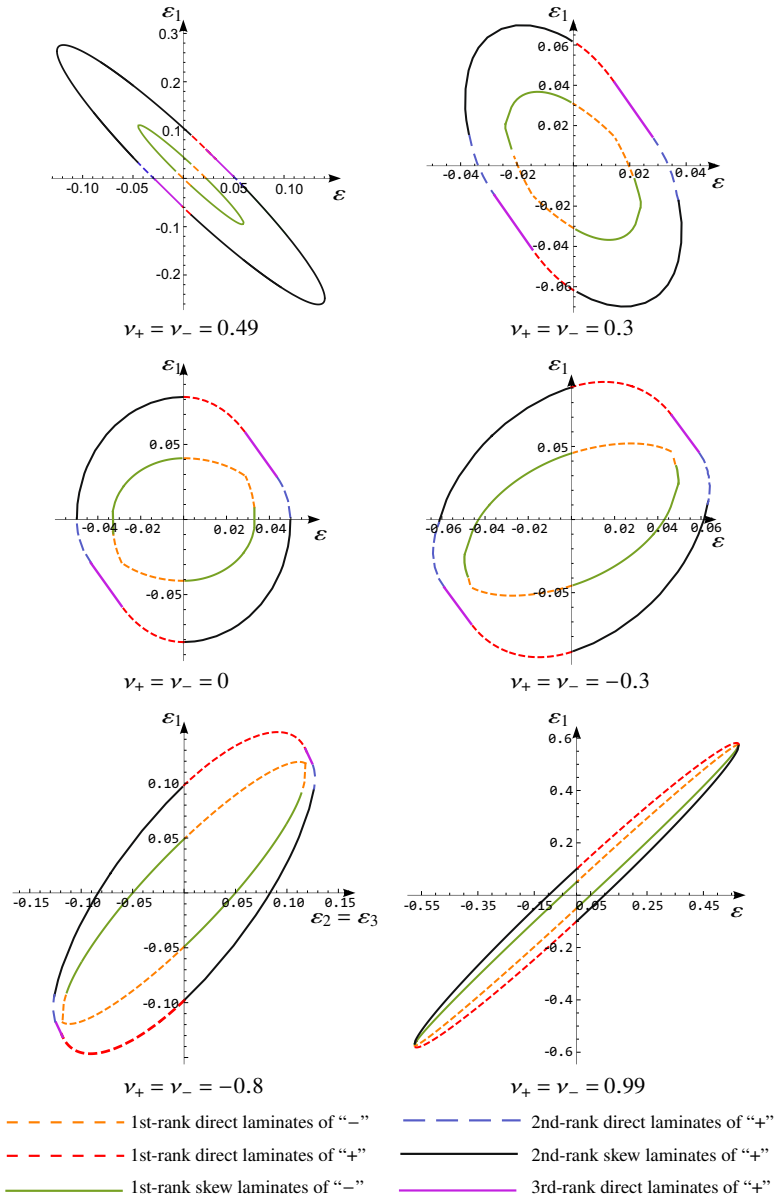

Fig. 15.7: Limiting surfaces for direct and reverse phase transformations in normal materials and auxetics. Initial state is phase "+".

for limiting surfaces construction for phase transformations 'auxetic ↔ normal material' and 'auxetic ↔ auxetic'.

We studied qualitatively and quantitatively how the sign and value of Poisson's ratio affect the conditions for switching the regimes corresponding to various laminates and change the shape of the limiting surface, and its orientation with respect to strain axes. We demonstrated that the construction of the PTZ and phase transformations limiting surfaces may be a tool for predicting the behavior of materials undergoing phase transformations and selecting material parameters.

Appendix. Maximal and minimal values of $F(N_1, N_2)$

This is a simple exercise to find the normals corresponding to maximal and minimal values of $F(N_1, N_2)$, depending on relationships between eigenvalues q_1, q_2, q_3. Results for $\nu > 0$ were presented earlier (see e.g. [53, 66, 60] or recent papers [45, 46, 47]). Nevertheless, for convenience, we give derivations here, highlighting the cases $\nu > 0$ and $\nu < 0$.

Let $\boldsymbol{q} = \sum q_k \boldsymbol{e}_k \boldsymbol{e}_k$, $n_k = \boldsymbol{n} \cdot \boldsymbol{e}_k$, $p_k = n_k^2$. To find the normal $\boldsymbol{n}^{ex}$ maximizing the function

$$F(N_1, N_2) = N_2 - aN_1^2, \quad a = \frac{1}{2(1-\nu)} \tag{A-1}$$

$$N_1 = \Sigma q_k p_k, \quad N_2 = \sum q_k^2 p_k, \quad \sum p_k = 1, \quad 0 \le p_k \le 1 \tag{A-2}$$

we take the Lagrange function

$$\Phi = F(N_1, N_2) - \lambda \Sigma p_k \tag{A-3}$$

where λ is the Lagrange multiplier.

From the conditions

$$\frac{\partial \Phi}{\partial p_k} = q_k^2 - 2aN_1 q_k - \lambda = 0, \quad k = 1, 2, 3 \tag{A-4}$$

it follows

$$q_1^2 - 2aN_1 q_1 = q_2^2 - 2aN_1 q_2 = q_3^2 - 2aN_1 q_3 = \lambda. \tag{A-5}$$

Then

$$q_1^2 - q_2^2 = 2aN_1(q_1 - q_2),\ q_1^2 - q_3^2 = 2aN_1(q_1 - q_3),\ q_2^2 - q_3^2 = 2aN_1(q_2 - q_3). \tag{A-6}$$

If q_i are different, i.e. $q_1 \neq q_2$, $q_1 \neq q_2$, $q_2 \neq q_3$, then, by (A-6),

$$q_1 + q_2 = q_1 + q_3 = q_2 + q_3 = 2aN_1. \tag{A-7}$$

Eq. (A-7) can be satisfied only if $q_1 = q_2 = q_3$, which is the contradiction.

Thus, if q_i are different then (A-5) cannot be fulfilled, maximum and minimum of $F(N_1, N_2)$ are reached at the boundary of the domain $\sum p_k = 1, 0 \le p_k \le 1$, i.e. if

$p_1 = 0$ or $p_2 = 0$ or $p_3 = 0$. This corresponds to the analysis presented graphically in Section 2, see Fig 15.1. That is why let us order the eigenvalues of $\boldsymbol{q}$ such that $q_1 > q_2 > q_3$ and consider the normals such that $n_2 = 0$. Then

$$N_1 = (q_1 - q_3)p_1 + q_3, \quad N_2 = (q_1^2 - q_3^2)p_1 + q_3^2 \tag{A-8}$$

Then F becomes the function of p_1, and from the condition

$$\frac{dF}{dp_1} = 0 \tag{A-9}$$

it follows that the the extrema is achieved if

$$q_1 + q_3 - 2a\{(q_1 - q_3)p_1 + q_3\} = 0 \tag{A-10}$$

This corresponds to

$$N_1 = \frac{q_1 + q_3}{2a}, \quad N_2 = \frac{(q_1 + q_3)^2}{2a} - q_1 q_3 \tag{A-11}$$

$$F = \frac{(q_1 + q_3)^2}{4a} - q_1 q_3 = \frac{1 - \nu}{2}(q_1^2 + q^2) - \nu q_1 q_3 \tag{A-12}$$

Since

$$\frac{d^2 F}{dp_1^2} = -2a(q_1 - q_3)^2 < 0,$$

the extrema, if it is achieved, indeed, is the minimum.

From (A-10) it follows that

$$p_1 = \frac{(1 - \nu)q_1 - \nu q_3}{q_1 - q_3}. \tag{A-13}$$

Formula (A-13) defines the normal only if

$$0 \le \frac{(1 - \nu)q_1 - \nu q_3}{q_1 - q_3} \le 1 \tag{A-14}$$

Since $q_1 > q_3$, conditions (A-14) are equivalent to the inequalities

$$0 < (1 - \nu)q_1 - \nu q_3 < q_1 - q_3 \tag{A-15}$$

which can be rewritten as

$$A = (1 - \nu)q_1 - \nu q_3 > 0 = q_1 - \nu(q_1 + q_3), \tag{A-16}$$

$$B = \nu q_1 - (1 - \nu)q_3 > 0 = \nu(q_1 + q_3) - q_3. \tag{A-17}$$

Since $A - B = (1 - 2\nu)(q_1 + q_3)$, and $-1 < \nu < 0.5$, the following implications are valid

$$q_1+q_3>0 \quad \Longrightarrow \quad A>B, \quad \text{(A-16) follows from (A-17)},$$
$$q_1+q_3<0 \quad \Longrightarrow \quad A<B, \quad \text{(A-17) follows from (A-16)}.$$

Then the normal can be defined by (A-13) in two cases for which

$$q_1+q_3>0 \quad \text{and} \quad \nu(q_1+q_3)>q_3, \tag{A-18}$$

or

$$q_1+q_3<0 \quad \text{and} \quad \nu(q_1+q_3)<q_1. \tag{A-19}$$

First consider $\nu>0$.

If $q_1q_3<0$, then $q_1>0$, $q_3<0$ and one of the cases (A-18) or (A-19) is met.

If $q_1q_3>0$ and $q_1>q_3>0$, then only the case (A-18) can take place for which

$$\nu q_1-(1-\nu)q_3>0. \tag{A-20}$$

If $q_1q_3>0$ and $q_3<q_1<0$, then only the case (A-19) can take place for which

$$-\nu q_3-(1-\nu)q_1>0 \tag{A-21}$$

that is equivalent to

$$\nu|q_3|-(1-\nu)|q_1|>0. \tag{A-22}$$

Finally obtain (15.26): the normal is defined at $\nu>0$ by (A-15) if

$$q_1q_3<0 \tag{A-23}$$
$$\text{or} \quad \{q_1q_3>0 \quad \text{and} \quad \nu|q|_{\max}-(1-\nu)|q|_{\min}>0\} \tag{A-24}$$
$$|q|_{\max}=\max\{|q_1|,|q_3|\}, \quad |q|_{\min}=\min\{|q_1|,|q_3|\} \tag{A-25}$$

Consider now $\nu<0$. From both (A-18) and (A-19) it follows that $q_1>0$, $q_3<0$, i.e. $q_1q_3<0$. Then from (A-18) it follows that

$$\nu q_1-(1-\nu)q_3>0,$$

and from (A-19) it follows that

$$-\nu q_3+(1-\nu)q_1>0.$$

Both inequalities can be rewritten in a unified form (15.27):

$$q_1q_3<0, \quad \nu|q|_{\max}+(1-\nu)|q|_{\min}>0 \tag{A-26}$$

The case of the axisymmetric $\boldsymbol{q}$ can be considered analogously.

Acknowledgements Authors acknowledge the financial support of the Russian Science Foundation (Grant No. 19-19-00552–П)

References

[1] Love AEH (1994) A Treatise on the Mathematical Theory of Elasticity, 4th ed, New York, Dover.
[2] Kolpakov AG (1985) Determination of the average characterisitics of elastic frameworks, PMM USSR **49**(6):739–745.
[3] Almgren RF (1985) An isotropic three-dimensional structure with Poisson's ratio= −1, J. Elasticity **15**:427–430.
[4] Lakes R (1987) Foam structures with a negative Poisson's ratio, Science **235**:1038–40.
[5] Evans KE, Nkansah MA, Hutchinson IJ, Rogers SC (1991) Molecular network design, Nature **353**:124–124.
[6] Lakes RS, Elms K (1993) Indentability of conventional and negative Poisson's ratio foams, Journal of Composite Materials **27**:1193–1202.
[7] Lakes RS (1993) Design considerations for negative Poisson's ratio materials, Journal of Mechanical Design **115**:696–700.
[8] Bezazi A, Scarpa F (2007) Mechanical behaviour of conventional and negative Poisson's ratio thermoplastic polyurethane foams under compressive cyclic loading, International Journal of Fatigue **29**(5):922–930.
[9] Bezazi A, Scarpa F (2009) Tensile fatigue of conventional and negative Poisson's ratio open cell PU foams, International Journal of Fatigue **31**(3):488–494.
[10] Scarpa F, Tomlinson G (2000) Theoretical characteristics of the vibration of sandwich plates with in-plane negative Poisson's ratio values, Journal of Sound and Vibration **230**:45–67.
[11] Greaves GN, Greer AL, Lakes RS, Rouxel T (2011) Poisson's ratio and modern materials, Nature Mater. **10**(11):823–37.
[12] Saxena KK, Das R, Calius E.P. (2016) Three decades of auxetics research – materials with negative Poisson's ratio: a review, Adv. Eng. Mater. **18**:1847–1870.
[13] Saadatmand S, Rasoulian A, Ashjari M (2017) Auxetic materials materials with negative poisson's ratio, Material Sci & Eng Int J. **1**(2):62–64.
[14] Lakes RS (2017) Negative-Poisson's-Ratio Materials: Auxetic Solids, Annu. Rev. Mater. Res. **47**:1.1–1.19.
[15] Ren X, Das R, Tran P, Ngo TD, Xie YM (2018) Auxetic metamaterials and structures: a review, Smart Mater. Struct. **27**:023001.
[16] Yang W, Li ZM, Shi W, Xie B-H, Yang M-B (2004) Review on auxetic materials. Journal of Materials Science **39**:3269–3279.
[17] Mir M, Ali MA, Sami J, Ansari U (2014) Review of Mechanics and Applications of Auxetic Structures, Advances in Materials Science and Engineering **2014**:753496.
[18] Lim T-C (2015) Auxetic Materials and Structures, in: Engineering Materials, Springer, Singapore.
[19] Hu H, Zhang M, Liu Y (2019) Auxetic Textiles. Woodhead, Duxford
[20] Lim T-C (2020) Mechanics of Metamaterials with Negative Parameters, in Engineering Materials, Springer, Singapore.

[21] Cui TJ, Smith DR, Liu R (Eds.) (2010) Metamaterials, Springer, New Yourk.
[22] Lakes R (2020) Composites and Metamaterials, World Scientific, New Jersey.
[23] Ko J, Bhullar SK, Mohtaram NK, Willerth SM, Jun MBG (2014) Using mathematical modeling to control topographical properties of poly (ε-caprolactone) melt electrospun scaffolds, Journal of Micromechanics and Microengineering **24**(6):1–13.
[24] Ali M, Busfield JC, Rehman I (2014) Auxetic oesophageal stents: structure and mechanical properties, Journal of Materials Science: Materials in Medicine **25**(2):527–553.
[25] Miller W, Ren Z, Smith CW, Evans KE (2012) A negative Poisson's ratio carbon fibre composite using a negative Poisson's ratio yarn reinforcement, Composites Science and Technology **72**(7):761–766.
[26] Evans KE (1991) Auxetic polymers: a new range of materials, Endeavour **15**(4):170–174.
[27] Sanamia M, Ravirala N, Alderson K, Alderson A (2014) Auxetic materials for sports applications, Procedia Engineering **72**:453–458.
[28] Duncan O, Shepherd T, Moroney C, Foster L, Venkatraman PD, Winwood K, Allen T, Alderson A (2018) Review of Auxetic Materials for Sports Applications: Expanding Options in Comfort and Protection, Applied Sciences **8**(6):941.
[29] Sloan MR, Wright JR, Evans KE (2011) The helical auxetic yarn - a novel structure for composites and textiles; geometry, manufacture and mechanical properties, Mech. Mater. **43**(9):476–486.
[30] Wang Z, Hu H (2014) Auxetic wrap-knitted spacer fabrics, Physica Status Solidi **251**(2):281–288.
[31] Lei M, Hong W, Zhao Z, Hamel C, Chen M, Lu H, and Qi HJ (2019) 3D Printing of auxetic metamaterials with digitally reprogrammable shape, ACS Appl. Mater. Interfaces **11**(25):22768–22776.
[32] Alomaraha A, Masood SH, Sbarski I, Faisal B, Gao Z, Ruan D (2020) Compressive properties of 3D printed auxetic structures: experimental and numerical studies, Virtual and Physical Prototyping **15**(1):1-21.
[33] Choudhry NK, Panda B, Kumar S (2021) In-plane energy absorption characteristics of a modified re-entrant auxetic structure fabricated via 3D printing, Composites Part B: Engineering **228**:109437.
[34] dell'Isola F, Steigmann DJ (2020) Discrete and Continuum Models for Complex Metamaterials, Cambridge University Press, Cambridge.
[35] Girchenko AA, Eremyev VA, Altenbach H (2012) Interaction of a helical shell with a nonlinear viscous fluid, International Journal of Engineering Science **61**:53–58.
[36] Eremeyev VA, dell'Isola F, Boutin C, Steigmann D (2018) Linear pantographic sheets: existence and uniqueness of weak solutions, J. Elasticity **132**:175–196.
[37] dell'Isola F, Seppecher P, Alibert JJ, Lekszycki T, Grygoruk R, Pawlikowski M, Steigmann D, Giorgio I, Andreaus U, Turco E, Gołaszewski M, Rizzi N, Boutin C, Eremeyev VA, Misra A, Placidi L, Barchiesi E, Greco L, Cuomo M, Cazzani A, Corte AD, Battista A, Scerrato D, Zurba IE, Rahali Y, Ganghoffer JF, Müller W, Ganzosch G, Spagnuolo M, Pfaff A, Barcz K, Hoschke K, Neggers

J, Hild F (2019) Pantographic metamaterials: an example of mathematically driven design and of its technological challenges, Continuum Mechanics and Thermodynamics **31**(4):851-884.

[38] Eremeyev VA, Turco E (2020) Enriched buckling for beam-lattice metamaterials, Mechanics Research Communications **103**:103458.

[39] Turco E, Barchiesi E, dell'Isola F (2022) A numerical investigation on impulse-induced nonlinear longitudinal waves in pantographic beams, Mathematics and Mechanics of Solids **27**(1):22–48.

[40] Stilz M, dell'Isola F, Giorgio I, Eremeyev VA, Ganzenmuller G, Hiermaier S (2022) Continuum models for pantographic blocks with second gradient energies which are incomplete, Mechanics Research Communications **125**:103988.

[41] Misra A, Hild F, Eremeyev VA (2023) Design of metamaterials: Preface, Mechanics Research Communications **127**:104036.

[42] Bianchi M, Scarpa F, Smith CW (2010) Shape memory behaviour in auxetic foams: Mechanical properties, Acta Materialia **58**:858–865.

[43] Wang W, He C, Xie L, Peng Q (2019) The temperature-sensitive anisotropic negative Poisson's ratio of carbon honeycomb, Nanomaterials **9**(4):487.

[44] Li Y, Wang S, Yang B (2021) Auxetic carbon honeycomb: strain-tunable phase transitions and novel negative Poisson's ratio, ACS Omega **6**:14896–14902.

[45] Antimonov MA, Cherkaev A, Freidin AB (2016) Phase transformations surfaces and exact energy lower bounds, Int. J. Engineering Sci. **98**:153–182.

[46] Freidin A, Sharipova L (2019) Two-phase equilibrium microstructures against optimal composite microstructures, Arch. Appl. Mech. **89**(3):561–580.

[47] Freidin A, Sharipova L, Cherkaev A (2021) On equilibrium two-phase microstructures at plane strain, Acta Mech. **232**:2005–2021.

[48] Cherkaev AV (2000) Variational Methods for Structural Optimization. New York, Springer-Verlag.

[49] Milton GW (2004) The Theory of Composites. Cambridge Monogr. Appl. Comput. Math. **6** Cambridge University Press, Cambridge.

[50] Chenchiah IV, Bhattacharya K (2008) The relaxation of two-well energies with possibility unequal moduli, Archive for Rational Mechanics and Analysis **187**(3):409–479.

[51] Freidin AB, Chiskis AM (1994) Regions of phase transitions in nonlinear-elastic isotropic materials. Part 1: Basic relations, Mech. Solid, **29**(4):91–109. Translated from Izvestia RAN, Mekhanika Tverdogo Tela **4**:91–109.

[52] Freidin AB (1999) Small strains approach to the theory on solid-solid phase transformations under the process of deformation, Studies on Elasticity and Plasticity (St. Petersburg State University) **18**:266–290 (in Russian).

[53] Morozov NF, Freidin AB (1998) Zones of phase transition zones and phase transformations in elastic bodies under various stress states, Proceedings of the Steklov Mathematical Institute **223**:219–232.

[54] Eremeev VA, Freidin AB, Sharipova LL (2003) Nonuniqueness and stability in problems of equilibrium of elastic two-phase bodies, Doklady Physics **48**:359–363.

[55] Yeremeyev VA, Freidin AB, Sharipova LL (2007) The stability of the equilibrium of two-phase elastic solids, Journal of Applied Mathematics and Mechanics **71**:61–84.
[56] Fu YB, Freidin AB (2004) Characterization and stability of two-phase piecewise-homogeneous deformation, Proc Roy Soc London Ser A **460**:3065–94.
[57] Grabovsky Y, Truskinovsky L (2011) Roughening instability of broken extremals, Archive for Rational Mechanics and Analysis **200**:183–202.
[58] Grabovsky Y, Truskinovsky L (2013) Marginal material stability, Journal of Nonlinear Science **23**:891–969.
[59] Freidin AB, Sharipova LL (2003) Equilibrium two-phase deformations and phase transitions zones within framework of small strains, Nonlinear problems of continuum mech. Izvestia Vuzov. North-Caucasus region. Special issue 291–299 (in Russian).
[60] Freidin A, Sharipova L (2006) On a model of heterogenous deformation of elastic bodies by the mechanism of multiple appearance of new phase layers, Meccanica **41**(3):321–339.
[61] Freidin AB, Vilchevskay EN, Sharipova LL (2002) Two-phase deformations within the framework of phase transition zones, Theor. Apll. Mech. **28–29**:149–172.
[62] Grinfeld M (1991) Thermodynamic Methods in the Theory of Heterogeneous Systems. Longman Sc & Tech.
[63] Kunin IA (1983) Elastic Media with Microstructure II. Springer-Verlag, Berlin, New York, etc.
[64] Kublanov LB, Freidin AB (1988) Solid phase seeds in a deformable material, Journal of Applied Mathematics and Mechanics (PMM USSR) **52**:382–389 (translated from Prikladnaia Matematica i Mekhanika (1988) **52**:493–501.
[65] Briane M (1994) Correctors for the homogenization of a laminate, Adv. Math. Sci. Appl. **2**:357–379.
[66] Freidin AB (2007) On new phase inclusions in elastic solids, Z Angew Math Mech (ZAMM) **81**(2):102–116.